

Design and synthesis of novel natural clinoptilolite-MnFe₂O₄ nanocomposites and their catalytic application in the facile and efficient synthesis of chalcone derivatives through Claisen-Schmidt reaction

Reza Aryan¹  · Noshin Mir¹ · Hamid Beyzaei¹ · Amin Kharade¹

Received: 1 December 2017 / Accepted: 1 March 2018
© Springer Science+Business Media B.V., part of Springer Nature 2018

Abstract A series of three novel nanocomposites were prepared by modifying the surface of natural clinoptilolite using various amounts of manganese ferrite (MnFe₂O₄) nanoparticles. These manganese ferrite-modified nanocomposites (MFO-NC) were fully characterized by XRD, FT-IR, EDX, VSM and TEM analyses. One of these novel nanocomposites with 40 wt% of manganese ferrite in clinoptilolite (MFO-NC-3) showed a strong catalytic behavior in the aldol-type Claisen-Schmidt reaction for the synthesis of chalcones. A strong catalytic synergy was observed between nano-MnFe₂O₄ particles and natural clinoptilolite in the structure of these nanocomposites. The products with a broad range of substituents on the reactants were efficiently obtained under room-temperature conditions within relatively short reaction times with good to excellent yields in the presence of one of the prepared MFO-NC nanocomposites. This nanocomposite also showed a strong stability and substantial reusability in the synthesis of chalcones.

Keywords Heterogeneous catalysis · Manganese ferrite · Natural clinoptilolite · Nanocomposite · Chalcones · Claisen-Schmidt reaction

Electronic supplementary material The online version of this article (<https://doi.org/10.1007/s11164-018-3366-4>) contains supplementary material, which is available to authorized users.

✉ Reza Aryan
rezaaryanchemist@yahoo.com; rezaaryan@uoz.ac.ir

¹ Department of Chemistry, Faculty of Science, University of Zabol,
P. O. Box: 9861335856, Zabol, Iran

Introduction

As iron-containing materials, MFe_2O_4 ($M=Co, Mn, Ni, Cu, \text{etc.}$), are very important substances with magnetic properties which have been widely studied for numerous applications [1, 2]. Among ferrites, $MnFe_2O_4$ nanoparticles have been widely used for magnetic resonance imaging technology and other electronic applications [3–7]. Furthermore, this material with its complex system [8] can also be applied for catalytic purposes as a heterogeneous catalyst [9–11] and for photodegradation of dyes [12, 13]. In spite of the high surface areas and abundant Lewis acidic reaction sites of ferrite nanoparticles [10], in order to decrease the manufacturing cost, increase the reusability potential and also prevent the possible toxicity of the applied nanocatalysts, there is a growing interest in using a natural porous substrate for hosting the nanoparticles. Natural clinoptilolite has recently been the subject of many studies as an abundant, cost-effective, and eco-friendly catalyst with a high surface area [14–16].

So far, various materials have been embedded in clinoptilolite structures for various applications. Depending on the employed material, the resulting composite has different properties. Clinoptilolite functions as a porous substrate which hosts the nanomaterial and improves its efficiency. Compared to other modified clinoptilolites [17–19], $MnFe_2O_4$ -clinoptilolite is a non-toxic and stable material having good Lewis acid properties which make it an excellent candidate for catalytic industrial applications. Moreover, it can be easily separated by an external magnetic field. The synthetic procedure of this nanocatalyst, on the other hand, should be precisely controlled to avoid unwanted possible impurities including iron and manganese oxide materials.

Chalcone derivatives have played a very important role in organic chemistry as important building blocks with a wide range of biological and medicinal properties. Natural products having chalcone building blocks have been extracted showing antifungal (Fig. 1, compound 1) [20], antiviral (Fig. 1, compound 2) [21], antiprotozoal (Fig. 1, compound 3) [22] and antidiabetic activities (Fig. 1, compound 4) [23].

The Claisen–Schmidt reaction is the most important route toward chalcone derivatives through the C–C bond forming an aldol condensation between acetophenone and benzaldehyde derivatives. A literature survey of very recently published methods revealed a plethora of catalytic conditions which have been used

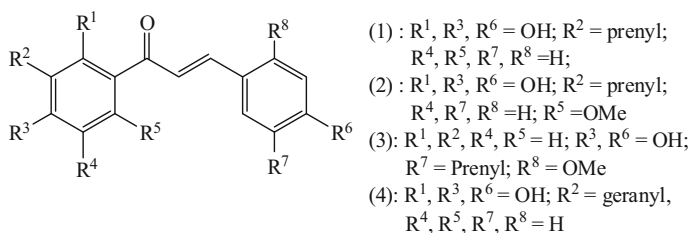


Fig. 1 Naturally occurring chalcone derivatives with valuable bioactivity effects

to promote this reaction, including the application of strong hydroxide bases and a wide variety of metallic catalysts in the presence of various solvents at different temperatures [24–36]. All these methods suffer from one or more serious drawbacks such as stepwise reaction conditions, demanding inert atmosphere, high reaction temperatures, long reaction times and limitations in the scope of the reactants. Therefore, novel heterogeneous catalysts are required so as to overcome these weaknesses.

According to the above-mentioned considerations and in continuation of our recent attempts to provide novel green media and catalysts for organic synthesis [37, 38], in the present study, MnFe_2O_4 -modified natural clinoptilolite (MFO–NC) was prepared and applied in the Claisen–Schmidt reaction for the synthesis of some chalcone derivatives. Although various types of modified clinoptilolite have been reported [39–43], to the best of our knowledge, this is the first time that manganese ferrite-modified clinoptilolite has been synthesized and applied as an efficient catalyst.

Experimental

Materials and characterization

The chemicals applied in this work were obtained from Fluka or Merck and used without further purification. Melting points of the products were recorded on a KRUSS type KSP1 N melting point meter apparatus and are uncorrected. FT-IR spectra were recorded on a Bruker Tensor-27 FT-IR spectrometer in KBr pellets. ^1H and ^{13}C NMR spectra were measured on a Bruker DRX-400 spectrometer, at 400 and 100 MHz, respectively, using TMS as an internal standard. Chemical shifts (δ) were reported relative to TMS, and coupling constants (J) were reported in Hertz (Hz). Mass spectra were recorded on a Shimadzu QP 1100 EX mass spectrometer with 70-eV ionization potential. Elemental analyses of the new compounds were performed with a Vario EL III 0 serial no. 11024054 instrument. X-ray diffraction (XRD) patterns were recorded by a Philips-X'PertPro X-ray diffractometer using Ni-filtered $\text{Cu K}\alpha$ radiation in a scan range of $10 < 2\theta < 80$. Fourier transform infrared (FT-IR) spectra were recorded on a Magna-IR, spectrometer 550 Nicolet with 0.125–1 cm resolution in KBr pellets in the range of 400–4000 cm^{-1} . TEM images were taken on an EM208S Philips transmission electron microscope with an accelerating voltage of 200 kV. Room-temperature magnetic properties were investigated using a vibrating sample magnetometer (VSM) device, made by Meghnatis Daghigh Kavir (Iran) in an applied magnetic field sweeping between ± 10000 Oe. Energy dispersive X-ray analysis (EDX) was performed by scanning electron microscopy (LEO-1455VP).

Synthesis of MFO–NC

In order to prepare the homoionic Na^+ -exchanged form of the clinoptilolite, the required amount of crude clinoptilolite was stirred in 2 M NaCl solution for about

24 h at 25 °C, and then the Na⁺-nanozeolite clinoptilolite was filtered off and washed twice with distilled water (50 mL). The Na⁺-nanozeolite was dried in an oven at 100 °C and then 5 g was poured into a 250-mL round-bottomed flask and 4 M sulfuric acid solution (100 mL) was added [44]. This mixture was heated at 80 °C for 1 h, allowed to cool, and then the activated nanozeolite precipitates were filtered off. The precipitates were washed with distilled water until complete neutralization and dried at 80 °C.

A homogeneous aqueous solution of 1 g CTAB in 100 ml distilled water was prepared by stirring for 10 min at 50 °C. This solution was transferred into a round-bottomed flask and 7 g activated nanozeolite was added to this solution. MnCl₂ (3 mmol) was then added at 80 °C under N₂ inert atmosphere and the mixture was stirred for 15 min at this temperature. Next, Fe₂(SO₄)₃·H₂O (3 mmol) was added to the reaction mixture under N₂ atmosphere and the reaction was heated at 100 °C for 15 min. Ammonium hydroxide was then added to the solution to reach a pH range of 13–14. The reaction mixture was stirred at 100 °C for another 2 h. Upon completion of the reaction, the solution was transferred to a Teflon-lined autoclave and heated at 250 °C for 4 h. After cooling, the obtained black precipitate was washed with deionized water and then dried at 100 °C for 12 h. Three modified nanozeolite catalysts with 10, 20, and 40 wt% of MnFe₂O₄ nanocrystals in clinoptilolite, denoted as MFO–NC-1, MFO–NC-2, and MFO–NC-3, respectively, were prepared. Pure MnFe₂O₄ was also prepared through similar methodology, except that no nanozeolite was used in the reaction flask.

General experimental approach for the preparation of chalcone derivatives catalyzed by MFO–NC-3

Acetophenone derivative (1 mmol), benzaldehyde derivative (1 mmol), MFO–NC-3 (0.06 g) were poured into a reaction tube containing an EtOH:water (1:1) mixture (2 ml) as solvent. The reactions were carried out at room temperature within relatively short times. TLC analysis was applied to monitor the reactions' progress (various mixtures of ethyl acetate and n-hexane as eluent). After completion of the reactions, the reaction mixture was vacuum-filtered off with a Büchi funnel and the catalyst was further washed with EtOH in order to complete the separation of the organic products. The organic layer was then poured onto ice and the chalcone precipitates were collected by vacuum filtration, dried at room temperature and recrystallized from the EtOH:water mixture whenever necessary.

Spectroscopic data for selected chalcone derivatives prepared in the present study (see Table 2 in "Results and discussion")

4-((E)-3-oxo-3-phenylprop-1-enyl)benzoxonitrile (Table 2, entry 1) IR (KBr): 3110, 2221, 1665, 1604 cm⁻¹. ¹HNMR (400 MHz, CDCl₃): δ 7.52–7.64 (m, 4H), 7.72–7.81 (m, 5H), 8.02 (d, *J* = 6.8 Hz, 2H).

(E)-3-(3-nitrophenyl)-1-phenylprop-2-en-1-one (Table 2, entry 3) IR (KBr): 3069, 1666, 1604 cm⁻¹. ¹HNMR (400 MHz, CDCl₃): δ 7.52–7.68 (m, 5H), 7.79–7.90 (m, 2H), 8.02–8.05 (m, 2H), 8.24 (d, *J* = 7.8 Hz, 1H), 8.49 (s, 1H).

(E)-3-(2,4-dichlorophenyl)-1-(3,4-dimethoxyphenyl)prop-2-en-1-one (Table 2, entry 7) IR (KBr): 3078, 3005, 2958, 2934 cm^{-1} . ^1H NMR (400 MHz, CDCl_3): δ 3.95 (s, 6H), 6.90 (d, $J = 10$ Hz, 1H), 7.27 (d, $J = 7.5$ Hz, 1H), 7.43–7.49 (m, 2H), 7.59–7.65 (m, 3H), 8.06 (d, $J = 15$ Hz, 1H).

(E)-3-(4-(benzyloxy)phenyl)-1-(3,4-dimethoxyphenyl)prop-2-en-1-one (Table 2, entry 9) IR (KBr): 3055, 2982, 2829, 2744, 1687, 1652, 1601 cm^{-1} . ^1H NMR (400 MHz, CDCl_3): δ 3.97 (s, 6H), 5.15 (s, 2H), 7.08 (d, $J = 8.5$ Hz, 2H), 7.37–7.42 (m, 6H), 7.84 (d, $J = 8.5$ Hz, 2H). ^{13}C NMR (100 MHz, CDCl_3): δ 55.9, 69.5, 112.7, 114.4, 114.8, 120.6, 123.6, 127.2, 127.9, 128.0, 128.2, 130.1, 132.9, 136.3, 143.7, 151.1, 154.3, 159.2, 187.3 ppm. MS (m/z): 374 (M^+). Elemental analysis $\text{C}_{24}\text{H}_{22}\text{O}_4$ Calculated: C, 76.99; H, 5.92; O, 17.09. Found: C, 76.53; H, 6.22; O, 17.25.

N-(4-((E)-3-(3,4-dimethoxyphenyl)-3-oxoprop-1-enyl)phenyl)acetamide (Table 2, entry 10) IR (KBr): 3350, 3091, 2987, 2936, 1691, 1642 cm^{-1} . ^1H NMR (400 MHz, CDCl_3): δ 2.21 (s, 3H), 3.97 (s, 6H), 6.92 (d, $J = \text{Hz}$, 1H), 7.25 (s, 1H), 7.52–7.80 (m, 8H) ppm. ^{13}C NMR (100 MHz, CDCl_3): δ 22.8, 57.6, 112.9, 114.0, 119.9, 120.6, 123.6, 129.5, 129.8, 132.4, 139.7, 145.1, 149.5, 155.6, 168.2, 188.1 ppm. MS (m/z): 325 (M^+). Elemental analysis $\text{C}_{19}\text{H}_{19}\text{NO}_4$ Calculated: C, 70.14; H, 5.89; N, 4.31; O, 19.67. Found: C, 69.72; H, 6.17; N, 4.75; O, 19.36.

(E)-3-(2,6-dichlorophenyl)-1-(4-nitrophenyl)prop-2-en-1-one (Table 2, entry 11) IR (KBr): 3104, 3078, 1665, 1598 cm^{-1} . ^1H NMR (400 MHz, CDCl_3): δ 7.23–7.26 (m, 1H), 7.38–7.41 (m, 2H), 7.64 (d, $J = 16$ Hz, 1H), 7.90 (d, $J = 16$ Hz, 1H), 8.14 (d, $J = 7.8$ Hz, 2H), 8.34 (d, $J = 7.8$ Hz, 2H) ppm. ^{13}C NMR (100 MHz, CDCl_3): δ 123.2, 124.9, 126.3, 128.8, 129.9, 132.2, 132.7, 135.1, 141.8, 152.5, 188.7 ppm. MS (m/z): 321 (M^+). Elemental analysis $\text{C}_{15}\text{H}_9\text{Cl}_2\text{NO}_3$ Calculated: C, 55.93; H, 2.82; Cl, 22.01; N, 4.35; O, 14.90. Found: C, 55.61; H, 3.11; Cl, 21.74; N, 4.76; O, 14.78.

(E)-3-(2,6-dichlorophenyl)-1-(4-fluorophenyl)prop-2-en-1-one (Table 2, entry 16) (KBr): 3101, 3063, 1663, 1601 cm^{-1} . ^1H NMR (400 MHz, CDCl_3): δ 7.28–7.31 (m, 1H), 7.38–7.46 (m, 2H), 7.63–7.67 (m, 3H), 7.86 (d, $J = \text{Hz}$, 2H), 8.10 (d, $J = 7.8$ Hz, 1H), ppm. ^{13}C NMR (100 MHz, CDCl_3): δ 115.1, 115.4, 124.9, 126.2, 129.3, 130.8, 131.6, 131.9, 132.1, 134.4, 134.7, 135.0, 135.5, 161.8, 166.9, 189.2 ppm. MS (m/z): 295 (M^+). Elemental analysis $\text{C}_{15}\text{H}_9\text{Cl}_2\text{FO}$ Calculated: C, 61.04; H, 3.07; Cl, 24.02; F, 6.44; O, 5.42. Found: C, 60.79; H, 3.36; Cl, 23.8; F, 6.12; O, 5.93.

Results and discussion

The prepared magnetic MnFe_2O_4 -modified natural clinoptilolite nanocomposite was first characterized by XRD, FT-IR, EDX, VSM and TEM analyses (see Electronic Supporting Information, ESI). In order to characterize the phase and purity of the as-prepared products, X-ray diffraction patterns were used (Fig S1, ESI file). Figures S1a–S1c show the XRD pattern of three different samples after the one-pot hydrothermal reaction including MFO–NC-1, MFO–NC-2, and MFO–NC-3, respectively. It can be seen that a mixed phase of clinoptilolite and MnFe_2O_4 is formed in all the samples. Moreover, some weak peaks representative of $\alpha\text{-Fe}_2\text{O}_3$ impurity are also observed. The appearance of $\alpha\text{-Fe}_2\text{O}_3$ sometimes occurs,

especially when MnFe_2O_4 is accompanied by other modifying agents. For instance, Hu et al. [45] observed $\alpha\text{-Fe}_2\text{O}_3$ and $\beta\text{-MnO}_2$ when they tried to prepare modified MnFe_2O_4 . It occurs because the stoichiometry of the initial salts changes due to the interactions of a part of the precursor with the host sample.

The diffraction peaks corresponding to MnFe_2O_4 are in agreement with the mineral called Jacobsite with the JCPDS No. of 01-074-2403, a cubic crystal system, and Fd-3 m space group. The related peaks of the embedded MnFe_2O_4 nanocrystals located at $2\theta = 29.5^\circ, 34.1^\circ, 42.5^\circ, 45.9^\circ, 52.0^\circ, 55.1^\circ, 61.5^\circ, 64.0^\circ, 65.5^\circ,$ and 69.2° are related to (220), (311), (400), (331), (422), (333), (440), and (620), respectively. The XRD pattern of clinoptilolite crystallites are assigned to the JCPDS No. 39-1383 which is in agreement with the previous reports of the Iranian clinoptilolite from the Semnan region [41]. By tracking the intensities of the MnFe_2O_4 crystalline lines, it is obvious that, from Fig. S1a to S1c, the peaks are getting sharper, while, on the other hand, the lines of $\alpha\text{-Fe}_2\text{O}_3$ are getting weaker. This shows that higher amounts of iron and manganese concentration result in better crystallization of the MnFe_2O_4 phase in the clinoptilolite lattice.

For characterization of the surface chemistry and functional groups of the sample, FT-IR spectra of the three MFO-NC samples were recorded and are shown in Fig. S2a-d for natural clinoptilolite, MFO-NC-1, MFO-NC-2, and MFO-NC-3 samples, respectively. In all cases, the wide band at 3430 cm^{-1} is due to the vibration of the O-H...O hydrogen bond of Si-O(H)-Al. In addition, the bands appearing at 1636 and 1091 cm^{-1} are attributed to the deformation vibration of the absorbed water and the asymmetric valence vibrations in tetrahedral SiO_4 , respectively [46]. The bands observed in the range of $705\text{--}660\text{ cm}^{-1}$ are assigned to the vibrations of 4- and 6-membered rings in the zeolite structure [47]. It has been shown that, by entering transition metal oxides into zeolitic frameworks, the vibrations below 900 cm^{-1} may be shifted [41]. In Fig. S2a-d, it can be seen that the vibration at 471 cm^{-1} in the FT-IR spectrum of pure natural clinoptilolite (Fig. S2a) is shifted to higher wavenumbers after incorporation of MnFe_2O_4 into the zeolite structure. However, such shifts are not obvious for the peaks at 611 and 796 cm^{-1} . The peak at 471 cm^{-1} is related to the bending vibrations of Si-O or Al-O and the observed slight shift in this peak shows a change in the bond strength due to the incorporation of MnFe_2O_4 in the zeolite rings. The absorption bands of Mn-O and Fe-O bonds generally appear at $404, 502,$ and 556 cm^{-1} , respectively [48], which have overlapped with clinoptilolite peaks and are not clearly observed in these spectra.

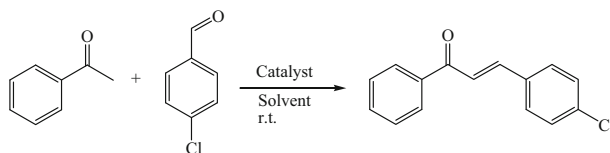
TEM images of natural clinoptilolite and MFO-NC (sample MFO-NC-3) are shown in Fig. S3a-S3b and S3c-S3d with different magnifications, respectively. In Fig. S3a-S3b, only the clinoptilolite structure is detected and no nanoparticles are observed in its structure. The similar contrast of the sample shows that the chemical structure is the same. For MFO-NC (Fig. S3c-S3d), in both images, it is clear that the MnFe_2O_4 nanoparticles with cubic and spherical shapes are embedded in the clinoptilolite layers. The size range of the nanoparticles was found to be $90\text{--}130\text{ nm}$ and they were not agglomerated. Different contrasts of nanoparticles and natural clinoptilolite show different chemical structure of the materials.

The elemental compositions of the samples were characterized by using EDX spectroscopy. Fig. S4a–c shows the EDX spectra of the MFO–NC-1, MFO–NC-2, and MFO–NC-3 samples, respectively. The presence of Si, Al, and O, which are from clinoptilolite and Fe, Mn, and O, due to the incorporation of MnFe_2O_4 nanoparticles are confirmed by EDX. It can be observed that the Fe:Mn ratios for the samples MFO–NC-1, MFO–NC-2 and MFO–NC-3 are 2.33, 2.26, and, 2.14, respectively.

VSM analysis was carried out for MFO–NC-1, MFO–NC-2, and MFO–NC-3 at room temperature and revealed ferromagnetic behavior of all the samples (Fig. S5, left). The measured values of saturation magnetization (M_s) were 3.55, 3.05, and 0.23 emu.g^{-1} and the remnant magnetization (M_r) values were 0.05, 1.44, and 1.52 emu.g^{-1} for MFO–NC-1, MFO–NC-2, and MFO–NC-3, respectively. These values are much lower than those of the reported bare MnFe_2O_4 particles ($M_s \sim 35 \text{emu.g}^{-1}$ and $M_r \sim 5 \text{emu g}^{-1}$) [49], which shows the effect of clinoptilolite in decreasing the magnetization of the product. The coercivities of the samples were 100.3, 190.2, and 122.6 Oe for MFO–NC-1, MFO–NC-2, and MFO–NC-3, respectively, which shows the resistance of the sample against demagnetization. These results show that the MFO–NC-2, and MFO–NC-3 samples are easily removed by an external magnetic field after the completion of the catalytic reaction. This fact is shown in Fig. S5, right, which demonstrates that that MFO–NC-1 was not removed by an external magnet even after 5 min. However, both MFO–NC-2, and MFO–NC-3 samples were easily separated by the magnet under 1 min.

The catalytic efficiency of the as-prepared MFO–NC nanocomposites was investigated in the Claisen–Schmidt reaction for the preparation of chalcone derivatives. The model reaction was performed using acetophenone (1 mmol), 4-chlorobenzaldehyde (1 mmol) and various catalysts including pure natural clinoptilolite, nano- MnFe_2O_4 and the three as-prepared MFO–NC nanocomposites (0.06 g) (Table 1) in the presence of various solvents at room temperature. (Scheme 1).

The model reaction did not proceed in the presence of MnFe_2O_4 and natural clinoptilolite as individual catalysts. The reaction was also slow in the presence of MnFe_2O_4 as the catalyst and a low yield of chalcone was obtained (Table 1, entry 1). The pure natural clinoptilolite showed less catalytic activity, and no sign of chalcone was observed even after 10 h (Table 1, entry 2), although a strong synergistic effect was established between the magnetic nano- MnFe_2O_4 and the natural clinoptilolite as the building components of nanocomposite catalysts MFO–NC-1 to MFO–NC-3 (Table 1, entries 3–9). For ferrites, the catalytic activity depends upon a variety of factors, such as the particle size, morphology and redox properties of metal ions and their distribution among the tetrahedral (A) sites and octahedral (B) sites of the cubic spinel lattice. The metal ions present in the octahedral sites play a crucial role in catalysis. This is because the octahedral sites are exposed on the surface. Mn^{3+} ions have a preference for the octahedral sites of the ferrite sub-lattice. The synergistic effect between the Fe–Mn ions present in the octahedral sites comes into play. [50] Therefore, the modification of the clinoptilolite surface by manganese ferrite nanoparticles provides a good opportunity for Mn^{3+} and Fe^{3+} ions to be better exposed to the reactants to use their Lewis



Scheme 1 Model Claisen–Schmidt reaction catalyzed by various novel clinoptilolite modified by manganese ferrite

Table 1 Optimization of the model Claisen–Schmidt reaction catalyzed by novel nanozeolite-modified manganese ferrite

Run No.	Catalyst ^a	Solvent ^b	Time (min.)	Yield (%) ^c	Comments
1	MnFe ₂ O ₄ (MFO)	EtOH:H ₂ O (1:1)	300	42	
2	Natural clinoptilolite (NC)	EtOH:H ₂ O (1:1)	600	–	Mixture of reactants and product
3	MFO–NC-3	EtOH	120	61	
4	MFO–NC-3	Water	720	–	Mixture of reactants and product
5	MFO–NC-3	DMF	300	67	
6	MFO–NC-3	No Solvent	330	54	
7	MFO–NC-1	EtOH:H ₂ O (1:1)	60	90	
8	MFO–NC-2	EtOH:H ₂ O (1:1)	45	93	
9	MFO–NC-3	EtOH:H ₂ O (1:1)	15	96	

^aCatalyst loading was 0.06 g per 1 mmol of benzaldehyde

^bAmount of solvent used was 2 ml per 1 mmol of benzaldehyde

^cIsolated yield

acidity and facilitate the formation of chalcone derivatives. Correspondingly, the MFO–NC-3 with the highest weight percentage of manganese ferrite nanoparticles is expected to show the best catalytic activity among these three nanocomposites (Table 1, entries 3–6 and 9). Moreover, as can be inferred from the TEM images of MFO–NC-3 as the most prosperous catalyst, modification of the natural clinoptilolite surface by MnFe₂O₄ inhibited the aggregation of the magnetic nanoparticles. This reasonably led to the maintaining of the high surface area of MnFe₂O₄ necessary for optimum catalytic activity and catalyst stability. The reaction times were significantly decreased and yields were considerably increased in the presence of these as-prepared catalysts. The reactions were also carried out in pure ethanol, water, dimethylformamide (DMF) and under solvent-free conditions in the presence of MFO–NC-3 catalyst. In the case of water as solvent, the reaction was not completed even after 12 h and the TLC analysis showed a mixture of reactants and

product (Table 1, entry 4). Under solvent-free conditions and in DMF as solvent, the model reaction proceeded slowly and moderate yields were obtained using MFO–NC-3 as the catalyst (Table 1, entries 5 and 6). The reaction was rather faster in pure ethanol as the solvent and using MFO–NC-3 as the catalyst, but the yield was still moderate. Using an ethanol:water (1:1) mixture as the solvent resulted in shorter reaction times and excellent yields (Table 1, entries 7–9). In these cases, the three MFO–NC catalysts were satisfactorily applied in the model reaction but the MFO–NC-3 showed a better catalytic activity by accomplishing the reaction within only 15 min and the best yield was obtained (Table 1, entry 9). Therefore, the MFO–NC-3 and ethanol:water (1:1) mixture were chosen as the best reaction conditions for the model reaction.

Next, catalyst loading was examined for the model reaction with various amounts of MFO–NC-3 in ethanol:water (1:1) at room temperature (Fig. 2). As indicated in Fig. 2, the higher amounts of MFO–NC-3 did not noticeably affect the reaction time and yield, while lower catalyst loading led to a slower reaction rate with similar yield. So, the amount of 0.06 g was chosen as the optimum amount of catalyst.

In order to examine the scope and generality of this novel catalytic protocol for the preparation of chalcone derivatives, various acetophenone and benzaldehyde derivatives possessing divergent electron demands were applied under the optimum reaction conditions (Scheme 2; Table 2; Fig. 3).

The results in Table 2 show a high electronic tolerance of the optimum catalyst for the present protocol. Electron-donating and electron-withdrawing substituents on the two reactants did not affect the rate and the facility of the process, and in all cases the products were prepared efficiently within short reaction times and good to excellent yields. Also, the products were easily separated from the catalyst by vacuum filtration using a Büchi funnel, and in many cases no further purification was needed.

A plausible mechanism has been proposed for the clarification of the role of the MFO–NC-3 nanocomposite as the catalyst in the synthesis of chalcones according to the above-mentioned considerations (Scheme 3). Both the acetophenone and benzaldehyde derivatives are activated by the dual Lewis acidic and Brønsted basic

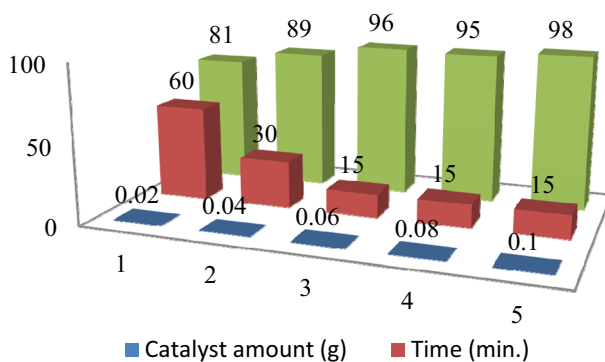
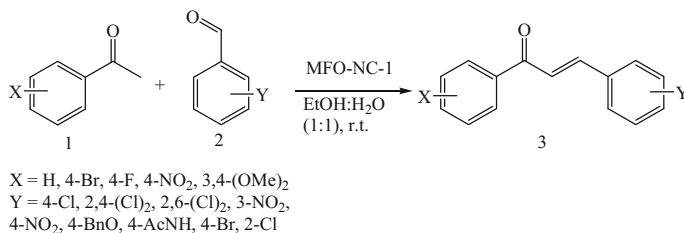


Fig. 2 Effect of MFO–NC-3 catalyst loading on the Claisen–Schmidt reaction. All reactions were performed using 1 mmol of the reactants in 2 ml of ethanol: water (1:1) at room temperature



Scheme 2 The scope and generality of MFO–NC-3-catalyzed synthesis of chalcone derivatives

Table 2 Synthesis of various chalcone derivatives using the MFO–NC-3 nanocomposite catalyst under optimized reaction conditions (Fig. 3)

Run no.	Product no.	Time (min.)	Yield (%) ^a	m.p. (°C)	Lit. m.p. (°C)
1	3a	30	88	150–153	151–153 [51]
2	3b	15	96	115–117	114–115 [52]
3	3c	15	93	155–157	159–162 [52]
4	3d	45	84	199–203	210–212 [52]
5	3e	20	87	169–172	–
	3f	10	95	161–162	–
6	3g	45	85	135–137	110–112 [53]
7	3h	30	89	138–140	132–135 [54]
8	3i	25	91	130–133	128 [55]
9	3j	15	94	79–81	–
10	3k	25	93	210–213	–
11	3l	25	83	148–150	–
12	3m	15	89	205–210	202–205 [56]
13	3n	30	88	186–188	183–185 [57]
14	3o	45	86	84–86	88–91 [54]
15	3p	45	85	85–86	102–103 [58]
16	3q	25	92	112–115	–

^aIsolated crude yields

features of nano-manganese ferrite supported on the surface of natural clinoptilolite. The enolate of acetophenone is formed in the presence of O²⁻ anions of MnFe₂O₄ as stronger nucleophilic species. Then, this enolate attacks the benzaldehyde derivative coordinated to the Fe⁺³ and Mn⁺² ions, leading to the formation of intermediate A, which undergoes dehydration to provide the desired chalcone derivative.

Subsequently, the catalyst reusability was examined in the model reaction as a significant factor in the application of novel heterogeneous catalysts. The nanocomposite catalyst MFO–NC-3 was filtered off the reaction medium after completion of the reaction, dried, and reapplied in the model reaction along with 4-chlorobenzaldehyde and acetophenone as reactants. The reaction was then carried out for 15 min at room temperature and the results are shown in Fig. 4.

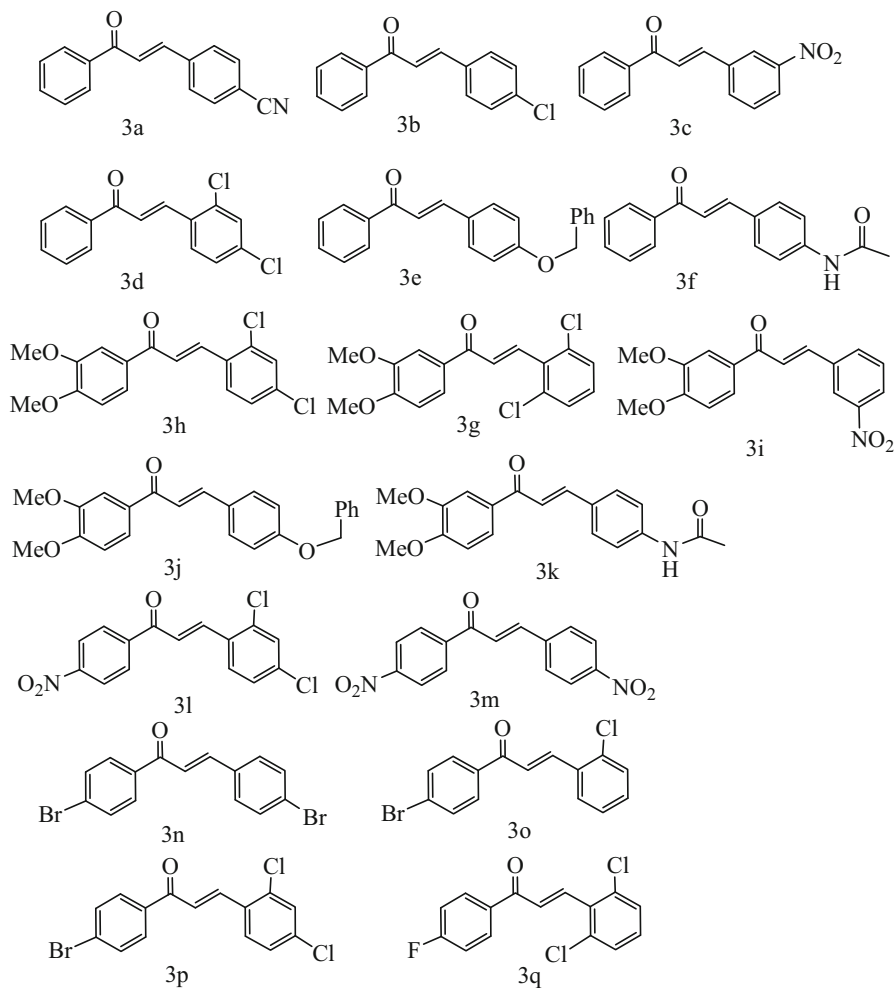


Fig. 3 The scope of the MFO-NC-3 catalyzed Claisen-Schmidt reaction

As indicated, only a slight loss of catalytic activity was observed after 4 reaction runs, which implies a good reusability of this novel catalytic system in catalysing the Claisen-Schmidt reaction.

Conclusion

A novel heterogeneous natural clinoptilolite-based catalyst was introduced by modifying the surface of natural clinoptilolite with various amounts of nano-manganese ferrite. These catalysts were characterized by XRD, FT-IR, EDX, TEM and VSM analyses. Then, the application of these catalysts was examined in the Claisen-Schmidt reaction for the synthesis of chalcones as a very important class of

Scheme 3 Proposed mechanism for the MFO–NC catalyzed Claisen–Schmidt reaction synthesis of chalcone derivatives

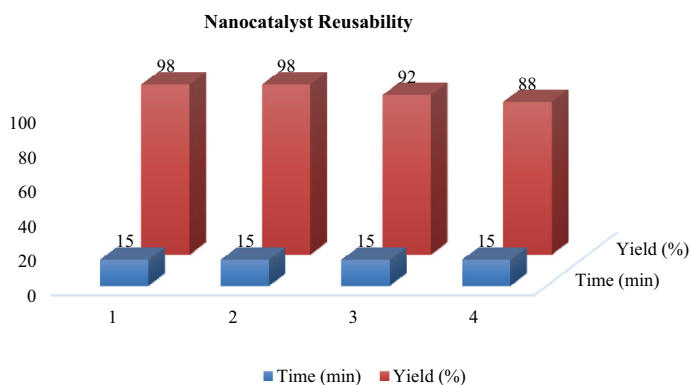
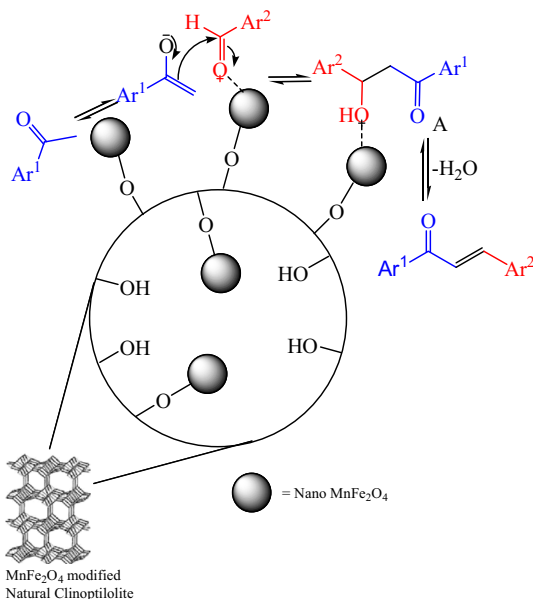


Fig. 4 Reusability of MFO–NC-3 catalyst in the model reaction for the synthesis of chalcones

organic building blocks with a wide range of applications. A strong synergistic collaboration was observed between the magnetic nano-MnFe₂O₄ and natural clinoptilolite as the building components of nanocomposite catalysts. Even though the MnFe₂O₄ and natural clinoptilolite individually failed to effectively promote the process, the reactions were successfully catalyzed by the as-prepared MFO–NC-3 nanocomposite having 40 wt% of MnFe₂O₄ relative to natural clinoptilolite at room temperature under mild conditions, achieving the desired products within short reaction times with good to excellent yields, and without any laborious purification method. The catalyst was easily collected and separated from the reaction mixture by an external magnet and vacuum filtration. The MFO–NC-3 catalyst also showed

valuable catalytic activities over a broad range of reactants with various electron demands and the corresponding chalcones were obtained with good to excellent yields. Moreover, the MFO-NC-3 showed a notable reusability and was repeatedly used four times with an infinitesimal loss of catalytic activity.

Acknowledgements The corresponding author gratefully acknowledges helpful scientific consultations from Dr. Masoomeh Nojavan. Partial financial support of this work by University of Zabol Research Council and the Dean of the Faculty of Science are also appreciated.

References

1. R.C. Pullar, *Prog. Mater. Sci.* **57**, 1191 (2012)
2. E. Casbeer, V.K. Sharma, X.Z. Li, *Sep. Purif. Technol.* **87**, 1 (2012)
3. G. Kulkarni, K. Kannan, T. Arunarkavalli, C. Rao, *Phys Rev B* **49**(724), 727 (1994)
4. J. Lu, S. Ma, J. Sun, C. Xia, C. Liu, Z. Wang, X. Zhao, F. Gao, Q. Gong, B. Song, *Biomater.* **30**, 2919 (2009)
5. U.I. Tromsdorf, N.C. Bigall, M.G. Kaul, O.T. Bruns, M.S. Nikolic, B. Mollwitz, R.A. Sperling, R. Reimer, H. Hohenberg, W.J. Parak, *Nano Lett.* **7**, 2422 (2007)
6. M.P. Leal, S. Rivera-Fernández, J.M. Franco, D. Pozo, M. Jesús, M.L. García-Martín, *Nanoscale* **7**, 2050 (2015)
7. V.G. Harris, A. Geiler, Y. Chen, S.D. Yoon, M. Wu, A. Yang, Z. Chen, P. He, P.V. Parimi, X. Zuo, J. Magn. Magn. Mater. **321**, 2035 (2009)
8. J.P. Chen, C.M. Sorensen, K.J. Klabunde, G.C. Hadjipanayis, E. Devlin, A. Kostikas, *Phys. Rev. B* **54**, 9288 (1996)
9. T. Valdés-Solís, P. Valle-Vigón, S. Álvarez, G. Marbán, A.B. Fuertes, *Catal. Commun.* **8**, 2037 (2007)
10. G. Brahmachari, S. Laskar, P. Barik, *RSC Adv.* **3**, 14245 (2013)
11. L. Menini, M.C. Pereira, L.A. Parreira, J.D. Fabris, E.V. Gusevskaya, *J. Catal.* **254**, 355 (2008)
12. P. Guo, G. Zhang, J. Yu, H. Li, X.S. Zhao, *Colloid Surf. A* **395**, 168 (2012)
13. B. Sahoo, S.K. Sahu, S. Nayak, D. Dhara, P. Pramanik, *Catal. Sci. Technol.* **2**, 1367 (2012)
14. Z. Özçelik, G.S.P. Soyulu, I. Boz, *Chem. Eng. J.* **155**, 94 (2009)
15. S.M. Baghbanian, N. Rezaei, H. Tashakkorian, *Green Chem.* **15**, 3446 (2013)
16. H. Choo, H.L. Kevan, *J. Phys. Chem. B* **105**, 6353 (2001)
17. S. Jafari, A. Nezamzadeh-Ejhi, *J. Colloid Interf. Sci.* **490**, 478 (2017)
18. J. Esmaili-Hafshejani, A. Nezamzadeh-Ejhi, *J. Hazard. Mater.* **316**, 194 (2016)
19. H. Sajjadi-Ghotbabadi, S. Javanshir, F. Rostami-Charati, *Catal. Lett.* **146**(338), 338 (2016)
20. H.N. El-Sohly, A.S. Joshi, A.C. Nimrod, L.A. Walker, A.M. Clark, *Planta Med.* **67**, 87 (2001)
21. V.E. Buckwold, R.J.H. Wilson, A. Nalca, B.B. Beer, T.G. Voss, J.A. Turpin, R.W. Buckheit, J. Wei, M. Wenzel-Mathers, E.M. Walton, R.J. Smith, M. Pallansch, P. Ward, J. Wells, L. Chuvala, S. Sloane, R. Paulman, J. Russell, T. Hartman, R. Patak, *Antivir. Res.* **61**, 57 (2004)
22. R. Sen, M. Chatterjee, *Phytomed.* **18**, 1056 (2011)
23. T. Enoki, H. Ohnogi, K. Nagamine, Y. Kudo, K. Sugiyama, M. Tanabe, E. Kobayashi, H. Sagawa, I. Kato, *J. Agric. Food Chem.* **55**, 6013 (2007)
24. M. Nasr-Esfahani, M. Daghighale, M. Taei, *J. Chin. Chem. Soc.* **64**, 17 (2017)
25. C.-B. Miao, Y.-M. Zeng, T. Shi, R. Liu, P.-F. Wei, X.-Q. Sun, H.-T. Yang, *J. Org. Chem.* **81**, 43 (2016)
26. F. Liu, J.-F. Yang, H. Liu, W.-Z. Wei, Y.-M. Ma, *J. Chin. Chem. Soc.* **63**, 254 (2016)
27. A.H. Jadhav, A.C. Lim, G.M. Thorat, H. Jadhav, J.G. Seo, *RSC Adv.* **6**, 31675 (2016)
28. C. Tamuly, I. Saikia, I.M. Hazarika, M. Bordoloi, N. Hussain, M.R. Das, K. Deka, *RSC Adv.* **5**, 8604 (2015)
29. S. Wu, X. Ma, J. Ran, Y. Zhang, F. Qin, Y. Liu, *RSC Adv.* **5**, 14221 (2015)
30. N. Kumar, L.S. Chauhan, C.S. Sharma, N. Dashora, R. Bera, *Med. Chem. Res.* **24**, 2580 (2015)
31. B.I. Roman, T. De Ryck, A. Patronov, H.S. Slavov, B.W.A. Van Hoecke, A.R. Katritzky, M.E. Bracke, C.V. Stevens, *Eur. J. Med. Chem.* **101**, 627 (2015)

32. M. Sugiura, Y. Ashikari, M. Nakajima, *J. Org. Chem.* **80**, 8830 (2015)
33. D. Rocchi, J.F. Gonzalez, C.J. Menendez, J. Carlos, *Molecules* **19**, 7317 (2014)
34. D. Kakati, N.C. Barua, *Tetrahedron* **70**, 637 (2014)
35. E.M. Schneider, R.A. Raso, C.J. Hofer, M. Zeltner, R.D. Stettler, S.C. Hess, R.N. Grass, W.J. Stark, *J. Org. Chem.* **79**, 10908 (2014)
36. M. Tiecco, R. Germani, F. Cardellini, *RSC Adv.* **6**, 43740 (2016)
37. R. Aryan, H. Beyzaei, M. Nojavan, T. Dianatipour, *Res. Chem. Int.* **42**, 4417 (2016)
38. R. Aryan, H. Beyzaei, M. Nojavan, M. Rezaei, *Res. Chem. Int.* **43**, 4731 (2017)
39. M. Saadat, A. Nezamzadeh-Ejhi, *Electrochim. Acta* **217**, 163 (2016)
40. H.B. Yener, M. Yılmaz, Ö. Deliismail, S.F. Özkan, Ş.Ş. Helvacı, *Sep. Purif. Technol.* **173**, 17 (2017)
41. H. Derikvandi, A. Nezamzadeh-Ejhi, *J. Mol. Catal. A: Chem.* **426**, 158 (2017)
42. F. Alidusty, A. Nezamzadeh-Ejhi, *Int. J. Hydrog. Energy* **41**, 6288 (2016)
43. Y. Huang, W. Wang, Q. Feng, F. Dong, *J. Saudi Chem. Soc.* **21**, 58 (2017)
44. S.M. Baghbanian, *RSC Adv.* **4**, 59397 (2014)
45. J. Hu, G. Chen, *Langmuir* **21**, 11173 (2005)
46. O. Korkuna, R. Leboda, J. Skubiszewska-Zie, T. Vrublevs'ka, V.M. Gun'ko, J. Ryczkowski, *Micropor. Mesopor. Mater.* **87**, 243 (2006)
47. E.M. Flanigen, H. Khatami, H.A. Szymanski, *Infrared Structural Studies of Zeolite Frameworks* (ACS publications, Washington, 1971)
48. S. Shafiu, R. Topkaya, A. Baykal, M.S. Toprak, *Mater. Res. Bull.* **48**, 4066 (2013)
49. M. Pal, R. Rakshit, K. Mandal, A.C.S. Appl. Mater. Interface **6**, 4903 (2014)
50. A. Goyal, S. Bansal, P. Samuel, V. Kumar, S. Singhal, *J. Mater. Chem.* **2**, 18848 (2014)
51. I. Kazi, S. Guha, G. Sekar, *Org. Lett.* **19**, 1244 (2017)
52. H. Samimi, H. Kiyani, Z. Shams, *J. Chem. Res.* **37**, 282 (2013)
53. Q. Chidan Kumar, B. Ching Kheng, H.K. Fun, S. Chandraru, M. Karabacak, *J. Mol. Struct.* **1116**, 135 (2016)
54. J.Z. Wu, J.L. Li, Y.P. Cai, Y. Pan, F. Ye, Y. Zhang, Y. Zhao, S. Yang, X. Li, G. Liang, *J. Med. Chem.* **54**, 8110 (2011)
55. M. Mehra, *J. Ind. Chem. Soc.* **33**, 618 (1956)
56. L. Gosney, *Tetrahedron* **29**, 1697 (1973)
57. Z. Gonda, Z. Novák, *Chem. Eur. J.* **21**, 16801 (2015)
58. F. Liu, J.F. Yang, H. Liu, W.Z. Wei, Y.M. Ma, *J. Chin. Chem. Soc.* **63**, 254 (2016)